

## ***Ab initio* study of spin-dependent transport in carbon nanotubes with iron and vanadium adatoms**

Joachim A. Fürst,<sup>1,\*</sup> Mads Brandbyge,<sup>1</sup> Antti-Pekka Jauho,<sup>1,2</sup> and Kurt Stokbro<sup>3</sup>

<sup>1</sup>*DTU Nanotech—Department of Micro- and Nanotechnology, NanoDTU, Technical University of Denmark, DK-2800 Kongens Lyngby, Denmark*

<sup>2</sup>*Department of Applied Physics, Helsinki University of Technology, P.O. Box 1100, FI-02015 HUT, Finland*

<sup>3</sup>*Department of Computer Science, Universitetsparken 1, DK-2100 Copenhagen Ø, Denmark*

(Received 28 January 2008; revised manuscript received 7 August 2008; published 5 November 2008)

We present an *ab initio* study of spin-dependent transport in armchair carbon nanotubes with transition metal adsorbates: iron or vanadium. The method based on density functional theory and nonequilibrium Green's functions is used to compute the electronic structure and zero-bias conductance. The presence of the adsorbate causes scattering of electrons of mainly one spin type. The scattering is shown to be due to a coupling of the two armchair band states to the metal *3d* orbitals with matching symmetry, giving rise to Fano antiresonances appearing as dips in the transmission function. The spin type (majority or minority) being scattered depends on the adsorbate and is explained in terms of *d*-state filling. We contrast the single-walled carbon nanotube results to the simpler case of the adsorbate on a flat graphene sheet with periodic boundary conditions and corresponding width in the zigzag direction, where the *d*-orbital selectivity is easily understood in terms of a simple tight-binding model.

DOI: [10.1103/PhysRevB.78.195405](https://doi.org/10.1103/PhysRevB.78.195405)

PACS number(s): 73.63.Fg

### **I. INTRODUCTION**

Various carbon structures have attracted considerable attention due to their potential use within future nanodevices.<sup>1</sup> Graphene, the single-atom-thick two-dimensional sheet of graphite, is the basis for many carbon materials. Rolling up such a sheet creates the one-dimensional single-walled carbon nanotube (SWNT) and wrapping up a sheet makes zero-dimensional (0D) fullerenes. These materials have a wide range of remarkable electronic properties. These include extremely high electron mobility found in suspended sheets of graphene.<sup>2</sup> Transistors have been fabricated based on SWNT with superior properties,<sup>1</sup> and more recently graphene ribbons—cut graphene sheets—were used to make a transistor,<sup>3</sup> which is stable at room temperature. These systems can also display a high surface sensitivity to atoms and molecules, which has led to ground-breaking applications such as micrometer-sized sensors capable of detecting single molecules.<sup>4</sup>

Not only pushing the limits within electronics, these carbon materials may lay the ground for the emerging field of spintronics,<sup>5–8</sup> where the functionality of the device is based on the spin degree of freedom. While graphene and SWNTs are not inherently magnetic, introducing defects,<sup>9–11</sup> impurities, or boundaries<sup>12,13</sup> may alter this fact. In recent years several studies have been carried out on SWNT or graphene-transition metal adatom systems. First-principles calculations have been employed to determine equilibrium geometries and magnetic properties: Fagan *et al.*<sup>14</sup> reported electronic structure studies on single iron<sup>14–16</sup> and manganese adatoms<sup>14,15</sup> on zigzag SWNTs, showing a total magnetic moment of the systems and in most cases a magnetization of the tube itself. A similar earlier study with additional transition metal elements on graphene was published by Duffy *et al.*<sup>17</sup> and later Mao *et al.*,<sup>18</sup> reaching similar conclusions. Manganese dimers, trimers, and wires on zigzag SWNTs<sup>15</sup>

exhibit magnetic moments close to free manganese. Yang *et al.*<sup>19</sup> proposed that iron- and cobalt-coated and -filled SWNTs can work as spintronic devices demonstrating a spin polarization close to 90% at the Fermi level, as well as considerable magnetic moments. Interestingly, both semiconducting and metallic SWNTs showed a high spin polarization. Kang *et al.*<sup>20</sup> obtained similar conclusions for various iron nanowire configurations inside armchair nanotubes.<sup>20</sup> On the other hand, work by Kishi *et al.*<sup>21</sup> shows that wires of iron and cobalt lose their magnetic moments when adsorbed on armchair SNWTs.

Filling of SWNTs with transition metals has been realized experimentally several years ago,<sup>22</sup> which adds to the potential of these systems. A few studies have been published on electron transport in this context. Iron-SWNT junctions with C<sub>60</sub> molecules<sup>23</sup> and pristine SWNTs<sup>24</sup> have been proposed as magnetic tunnel junctions. First-principles transport calculations yield tunnel magnetoresistances of 11% and 40%, respectively, for these systems. A spin-polarized current has also been reported in theoretical works on nanoribbons with substitutional boron atoms,<sup>25</sup> where spin-dependent scattering is found. Recently, Rosales *et al.*<sup>26</sup> studied graphene nanoribbons with organic molecules adsorbed at the ribbon edge using tight binding, and found Fano antiresonances in the conductance.

Motivated by the reported spin-dependent scattering, we here investigate the influence on the transport properties of a single iron or vanadium atom adsorbed on armchair SWNTs. By performing *ab initio* spin-polarized transport calculations we demonstrate a spin-dependent scattering and show how the spin type being scattered is related to the type of adsorbate. By analyzing the projected density of states (PDOS) onto the *3d* orbitals of the adsorbates, we find the scattering to be caused by coupling of the SWNT band states to these orbitals, resulting in Fano antiresonance phenomena. Using a simple tight-binding model we qualitatively reproduce these results.

The paper is organized as follows. In Sec. II we introduce the method and a simple model system for the SWNT. It consists of a graphene sheet with periodic boundary conditions (GPB) transverse to the transport direction. The GPB system is relatively small and neglects curvature effects, which allows for an easier analysis of the scattering. The results for the GPB system will be used throughout the paper as a reference to which we can compare the results for the larger and much more demanding SWNT systems. We describe the relaxation and relaxed geometries in Sec. III for the GPB and SWNT systems. The *ab initio* transport results for the GPB system are presented in Sec. IV and the Fano resonance is briefly introduced along with a transmission eigenchannel analysis. Next, these results are compared to a tight-binding model in Sec. V considering the symmetries of the *d* orbitals and the carbon band states at the Fermi energy. Results from *ab initio* calculations on the (10,10) SWNT systems are given in Sec. VI, where we demonstrate that the scattering mechanism as understood for the GPB system also applies to these more realistic systems. In addition, a direct comparison between (10,10) SWNT and corresponding GPB systems is presented. We finally conclude in Sec. VII.

## II. METHOD AND SYSTEMS

We have used the *ab initio* pseudopotential density functional theory (DFT) as implemented in the SIESTA code<sup>27</sup> to obtain the electronic structure and relaxed atomic positions from spin-polarized DFT. We employ the generalized gradient approximation (GGA) pseudopotential for exchange-correlation.<sup>28</sup> Our spin-transport calculation is based on the nonequilibrium Green's function method as implemented in the TRANSIESTA code,<sup>29</sup> extended to spin-polarized systems. However, we only consider here the zero-bias limit and focus on electron transmission close to the Fermi energy. The transmission is obtained from

$$T(\epsilon) = \text{Tr}[\Gamma_L(\epsilon)\mathbf{G}^a(\epsilon)\Gamma_R(\epsilon)\mathbf{G}^r(\epsilon)], \quad (1)$$

where the retarded Green's function,  $\mathbf{G}^r(\epsilon)$ , is calculated from the Hamiltonian and self-energies of the central region.  $\Gamma_\alpha(\epsilon)$  is the imaginary part of the self-energies (times two) of the left and right electrodes ( $\alpha=L,R$ ). The self-energies are computed recursively from the bulk Hamiltonian of the infinite electrodes, obtained by an initial bulk calculation of the electrodes.

In Fig. 1 we show the system setup used for transport calculations on the GPB system. The graphene sheet is cut in an armchair structure along the *y* direction, which results in a metallic system. We employ periodic boundary conditions in the transverse *x* direction to mimic the structure of a tube. According to the TRANSIESTA method<sup>29</sup> the system is divided into left and right electrodes, marked *L* and *R* in Fig. 1, and a central region marked *C*. A single iron or vanadium adatom is placed in the middle of the central region. In the case of the GPB system shown in Fig. 1 the period of the cell in the transverse *x* direction is 8.52 Å, which is then the smallest distance between adatoms in neighboring cells, and should be enough to prevent significant adatom-adatom interactions.<sup>30</sup> We employ Gamma point sampling ( $k=0$ ) in

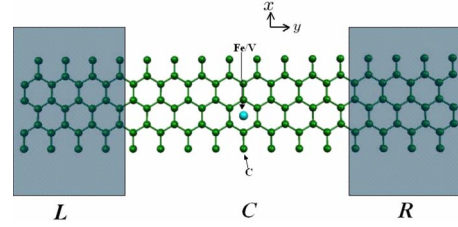


FIG. 1. (Color online) The unit cell of the GPB system. The sheet is cut in an armchair structure along the *y* direction. The adatom, iron, or vanadium is placed in the center. The shaded areas marked *L* and *R* are the electrodes, and *C* is the central region. Periodic boundary conditions are imposed in the transverse direction (*x*).

the periodic *x* direction. The GPB system then corresponds to a (2,2) armchair nanotube as described by the approximate graphene sheet model,<sup>31</sup> that is, neglecting curvature effects.

The electrodes of the GPB system both contain 32 atoms, while the central region consists of 64 sheet atoms. Such central region size ensures bulk density in the leads, which is crucial in the TRANSIESTA method. For the (10,10) SWNT systems we use electrodes consisting of 80 C atoms and a central region of 200 C atoms. The shorter central region compared to the GPB system is sufficient due to the enhanced screening of the iron or vanadium adatom. A unit-cell size in the *x* and *y* directions of 30 Å yields a tube-tube distance of 15 Å.

## III. RELAXATION AND GEOMETRIES

The systems are relaxed using the conjugate gradient method with a force tolerance of 0.01 eV/Å. The carbon atoms were kept fixed during geometry optimization. The mesh cutoff value defining the real-space grid used for relaxation for the GPB (SWNT) system is 400 Ry (200 Ry) and a double-zeta-polarized (single-zeta) basis set for the adatom. A single-zeta basis was used for carbon for all systems. (The difference in real-space grid between 400 Ry and 200 Ry results in relaxed adatom position differences of less than 0.05 Å.) The relaxed position of the adatoms is for all systems at the center of a hexagon. The distance of the iron (vanadium) atom to the four closest carbon atoms on the SWNT is 2.23 Å (2.40 Å). Yagi *et al.*<sup>30</sup> reported 2.41 Å for iron on a (4,4) SWNT. For the GPB system the relaxed distance of iron (vanadium) from the sheet plane is 1.77 Å (1.89 Å), corresponding to carbon-adatom distances of 2.25 and 2.37 Å. This is considerably different from the plane-wave results obtained by both Yagi *et al.*<sup>30</sup> and Mao *et al.*,<sup>18</sup> reporting heights of 1.51 and 1.47 Å for adsorption on graphene. Koleini *et al.*<sup>32</sup> reported vanadium heights of 1.7 Å using a double-zeta-polarized basis, which is also lower than ours. The differences are due to the small basis used in our work, where our focus is on the transport properties. Therefore, in Sec. IV we consider the sensitivity of the transport results with respect to adatom position, and conclude that the scattering is rather robust with respect to such geometry changes. Thus the mesh cutoff value for the trans-

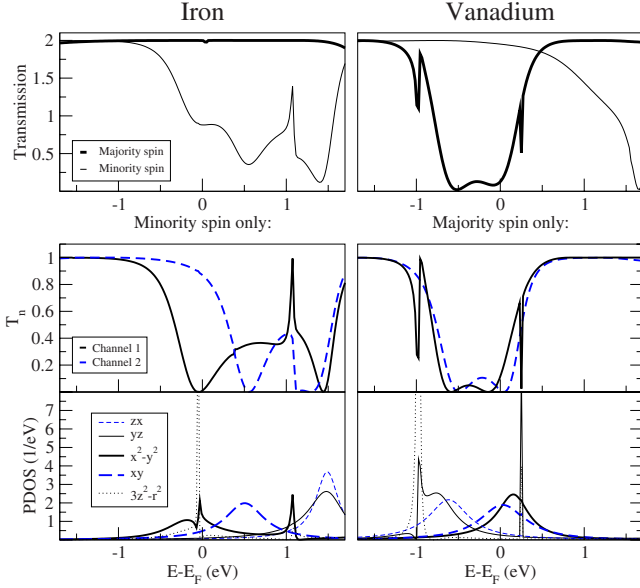


FIG. 2. (Color online) Top: Transmission as a function of energy for iron (left) or vanadium (right) on the GPB system. Within a 0.5 eV range of  $E_F$  the minority spin channels are suppressed in the case of iron, whereas the majority channels are suppressed for vanadium. Middle: The transmission of the two minority (majority) spin channels for the iron (vanadium) system. The sum of the two channels yields the total transmission in each case. Bottom: The projected density of states (PDOS) of the 3d orbitals of the iron (vanadium) adatom for minority (majority) spin.

port calculation was lowered to 175 Ry, and the basis reduced to single-zeta since the effect on the transmission was negligible.

#### IV. RESULTS FOR GPB SYSTEM

The spin-resolved transmissions as a function of energy relative to the Fermi level,  $E_F$ , of the GPB with iron and vanadium adatoms are shown in Fig. 2. The transmission of a pure sheet is two for each spin type since there are two bands in the energy window each contributing with a fully transmitting channel for each spin.<sup>31</sup> It is seen that spin-dependent scattering occurs due to the presence of the adatoms. In the case of iron the minority spin transmission is significantly suppressed around  $E_F$ , whereas the majority spin electrons transmit completely. For vanadium, likewise, scattering occurs for only one spin channel, but in this case it is the majority spin electrons which are scattered. The transmission of the two bands for minority (iron) and majority (vanadium) spin is shown on Fig. 2, middle graph. We see that each band closes completely at certain energies.

In the case of vanadium ( $3d^34s^2$ ) we expect from Hund's rules a total spin moment of  $3\mu_B$  and the majority  $d$  states will be located around  $E_F$ , whereas the minority states are all empty and well above  $E_F$ . The Mulliken analysis indicates a half filling of the majority spin  $3d_{yz}$  and  $3d_{zx}$  orbitals and a full filling of  $3d_{x^2-y^2}$ ,  $3d_{xy}$ , and  $3d_{3z^2-r^2}$ . For minority electrons all 3d orbitals are empty. This is in agreement with the 3d-orbital PDOS plot shown in Fig. 2 bottom graph. In the

case of iron ( $3d^64s^2$ ) we expect from Hund's rules that the majority states are all filled and well below  $E_F$ , and now the partially filled minority states are located around  $E_F$ , yielding a total spin moment of  $4\mu_B$ . This is again supported by the Mulliken analysis data, as well as the PDOS. The total spin of iron (vanadium) as obtained from the Mulliken analysis is 3.57(3.35) $\mu_B$ , which differs from the expected 4(3) $\mu_B$ . This is mainly due to charge transfer from the 4s orbitals to the 3d as also noted in Ref. 16. Additional filling of the minority (majority) spin 3d orbitals explains the decrease (increase) in total spin of iron (vanadium). This transfer is more enhanced for smaller adatom heights. For this reason, as well as the sensitivity of Mulliken data to basis set, the moments are higher than those reported by Refs. 30 and 18 for iron of  $2.1\mu_B$  and  $2.2\mu_B$ , respectively.

Comparing PDOS and the transmission there is a strong correlation between adatom orbital energies and conductance dips. This is very clear for the two separated channel closings for vanadium at  $E \approx E_F$  and  $E - E_F \approx -0.5$  eV. Similar PDOS plots for the adatom  $s$  orbitals do not show such correlation. The interference between waves involving the quasisubband  $d$  state on the adatom and directly transmitted band states yields a Fano antiresonance. The line shape of the resonance is given by the Fano function<sup>33</sup>

$$f(\epsilon) = \frac{(\epsilon + q)^2}{\epsilon^2 + 1}, \quad (2)$$

where  $\epsilon = (E - E_R)/\Gamma$ . Here  $\Gamma$  is the resonance width,  $E_R$  is the resonance energy, and  $q$  is the asymmetry parameter. Since the structure has inversion symmetry around the adatom in the transport direction, the parameter  $q$  must be real, and thus, we expect to have zero transmission dips as seen in Fig. 2 at the antiresonances  $\epsilon = -q$ .<sup>34,35</sup> A very sharp resonance can be seen for vanadium around  $-1$  eV, which is related to the  $3d_{yz}$  and  $3d_{3z^2-r^2}$  orbitals. The strong asymmetry of this dip shows that the special symmetric case of the Fano function—the Breit-Wigner line shape—does not apply here. In general, the Fano function applies since the line shape of the transmission follows the shape of the orbital PDOS, which, in general, is not symmetric. Signatures of Fano resonances have previously been observed experimentally in the conductance of multiwall carbon nanotubes at low temperature.<sup>36</sup>

In order to investigate the dependence of the scattering on adatom position we calculate the transmission for various heights ranging from those of this work obtained with a small basis set to those found in plane-wave calculations.<sup>18,30</sup> The results are shown in Fig. 3 in the case of iron for heights of 1.50 to 1.77 Å. The scattering mechanism is seen to be robust with respect to these very large changes of the adatom geometry. The minority spin is scattered more as the height is reduced. PDOS analysis reveals that the  $3d_{xy}$  orbital shifts downwards in energy due to larger filling, which causes scattering of both channels around the Fermi energy.

The antiresonances are illustrated further by performing an eigenchannel analysis, where scattering states with well-defined transmissions, so-called “eigenchannels,” are

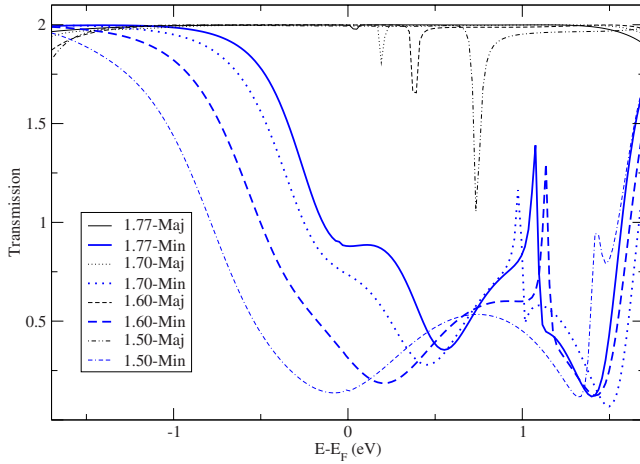


FIG. 3. (Color online) The transmission for the (2,2) GPB system for different iron adatom distances to the sheet plane ranging from 1.50 to 1.77 Å.

constructed.<sup>37</sup> We take vanadium as our example. The eigenchannel transmissions,  $T_n(\epsilon)$ , provide the transmission of channel  $n$  at a given energy  $\epsilon$ . Figures 4(a)–4(d) show for both bands the real part of the majority spin left to right scattering states for energies corresponding to the first dip (−0.5 eV) and the second dip (−0.1 eV), respectively. We see that the wave function is vanishing on the right side of the vanadium atom as expected since we have full reflection in all cases. We also see that the solutions are antisymmetric [Fig. 4(a) and 4(d)] or symmetric [Fig. 4(b) and 4(c)] with respect to a plane perpendicular to the  $x$  direction. In the transverse direction the neighboring C atoms have the same (opposite) sign in the symmetric (antisymmetric) case. These solutions are indeed matched by the vanadium atom orbitals, which are indicated on the figures by matching signs (col-

ors). From the shape and sign in the plots the orbitals involved can be identified for each band at both energies.

## V. TIGHT-BINDING MODEL

We will now rationalize the results for the channels and transmissions in terms of the simplest possible tight-binding model. We consider only the coupling of the adatom  $d$  orbitals with the six nearest  $\pi$  orbitals. The starting point will be the two band states of the  $\pi$  electrons in the armchair direction at the Fermi level (see Fig. 5). These are characterized by rotational symmetry in the  $x$  direction and come in an odd or even version around the symmetry plane  $y$  cutting through the adatom. They couple to different  $d$  orbitals on the adatom with the same symmetry. Thus the symmetric or antisymmetric band only couples to the  $d$  orbitals even or odd in  $x$ .

To make a model with a minimum number of parameters we assume that the  $d$  orbitals have the same on-site energy  $E_d$ , and a coupling to the carbon  $\pi$  orbitals described in units of  $V_{pd}=V_{pd\sigma}$  taking  $V_{pd\pi}\approx 0.5V_{pd\sigma}$ .<sup>38</sup> The size and sign of the coupling of the different  $d$  orbitals to the  $p_z$  orbitals are illustrated in Fig. 5, left and right panels corresponding to coupling to the two types of bands. For both bands it is seen that the  $3d_{3z^2-r^2}$  orbitals do not couple at  $E_F$  since the wavefunction values around the hexagon sum up to zero. Therefore, we do not expect significant contributions from this orbital, which will be very localized. Again, due to symmetry, the same argument holds for the  $s$  orbitals. We only consider the majority spin  $d$  states for V since they, as mentioned above, will be located around  $E_F$  with  $E_d\approx 0$ . Likewise, for iron we only consider the minority spin states. The results for the model calculation with  $(E_d, V_{pd})$  parameters chosen to fit the data from the full *ab initio* calculation are shown in Fig. 6, calculated by the same approach as outlined

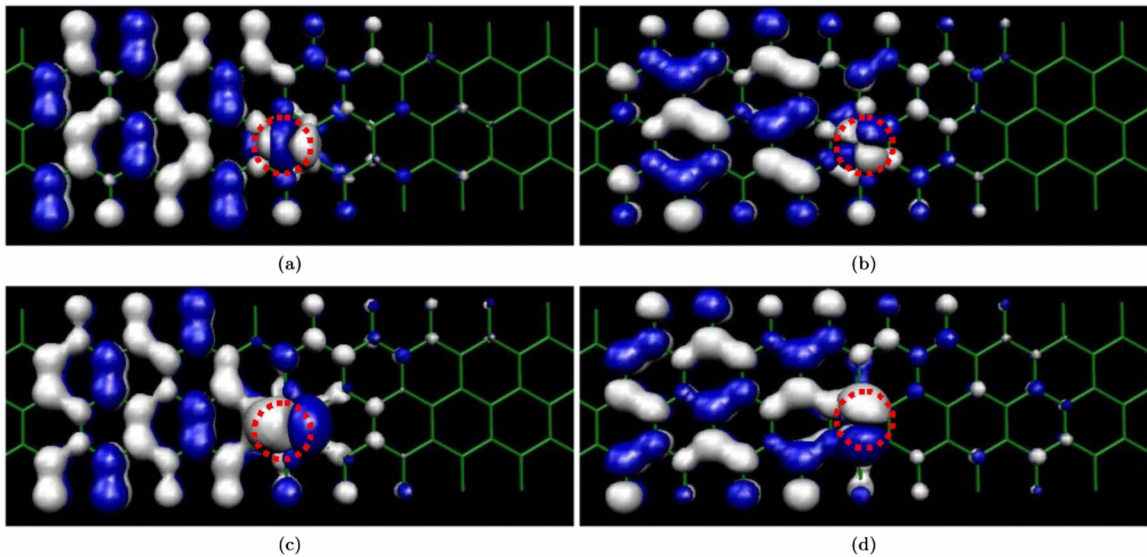


FIG. 4. (Color online) The real part of the (left-to-right) eigenchannel scattering states for the vanadium GPB system, stemming from majority spin electrons from both bands, at the energy of the first dip (−0.5 eV) [(a),(b)] and second dip (−0.1 eV) [(c),(d)] in the transmission spectrum. Only the solutions in the scattering region are shown. The size of the shapes indicates a cutoff value for the wave function. White indicates a positive sign and blue indicates a negative sign of the wave function. The involved orbitals of the vanadium atom (marked with dotted circle) are seen to be (a):  $3d_{x^2-y^2}$  (and a minor presence of  $3d_{3z^2-r^2}$ ); (b):  $3d_{xy}$ ; (c):  $3d_{yz}$ ; and (d):  $3d_{zx}$ .

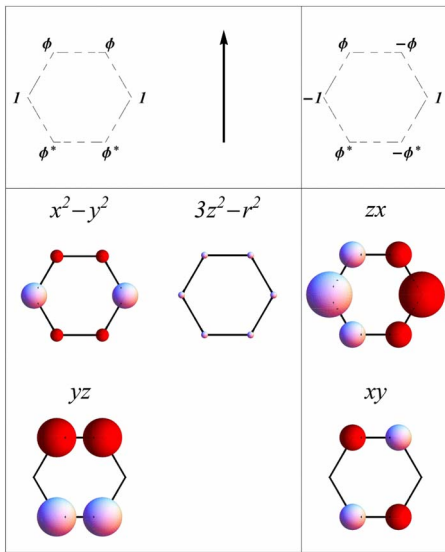


FIG. 5. (Color online) Top panel: The two  $\pi$ -band ( $p_z$ ) states (not normalized) in a hexagon where the arrow denotes the direction along the armchair GPB ( $y$  direction) with  $\phi=e^{i2\pi/3}$ . Left and right panel correspond to symmetric and antisymmetric solution on the A, B dimers ( $x$  direction). Lower panels: Simple tight-binding model. The sign and relative size of the hopping matrix elements between the ring  $\pi$  orbitals and the metal adatom  $d$  orbitals when the metal atom is situated 1.7 Å above the middle of the ring.

in Sec. II. It is seen that the transmission is more suppressed in the full calculation, where the individual  $d$  orbitals are allowed to have different energies, but the fact that we see four dips corresponding to the four coupling  $d$  orbitals is clear.

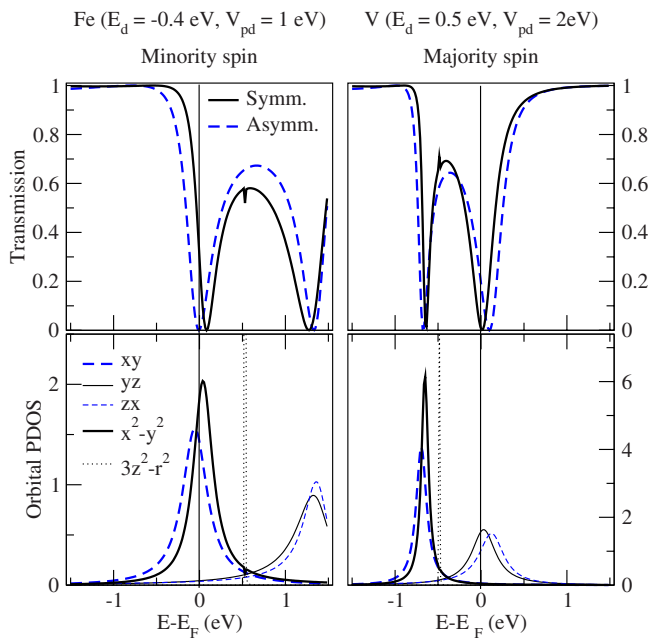


FIG. 6. (Color online) The transmission through the symmetric and antisymmetric bands for Fe minority spin (left panels) and V majority spin (right panels) calculated with the simple tight-binding model. Lower panels display the projected density of states onto the  $d$  orbitals.

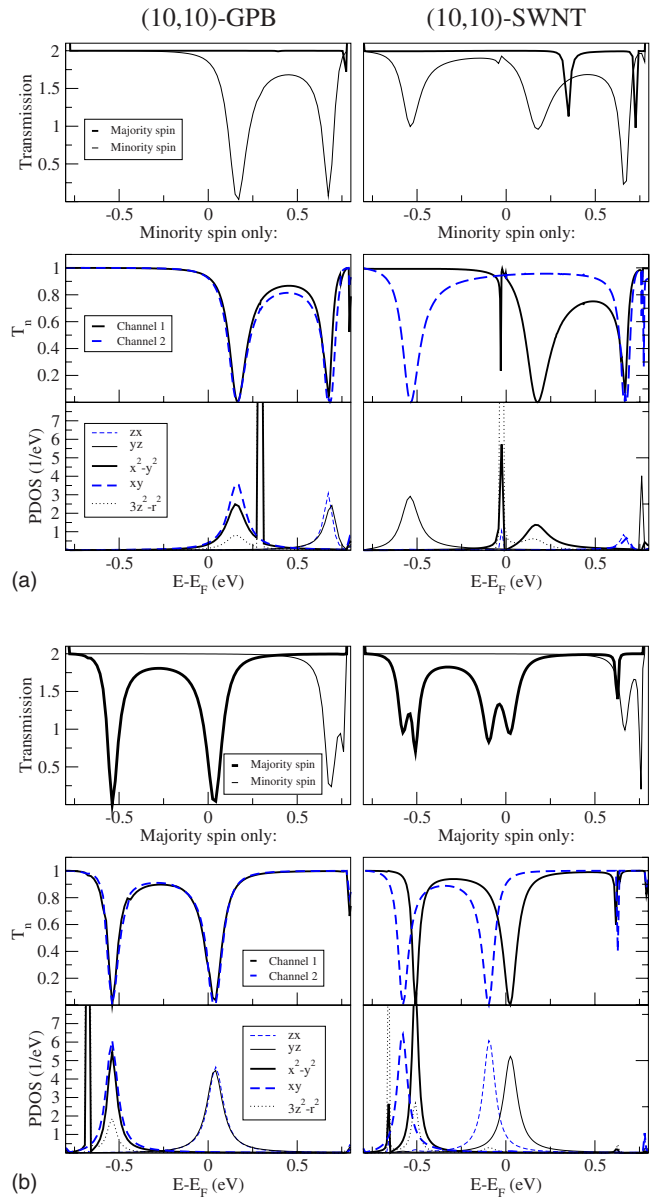


FIG. 7. (Color online) An analysis as the one given in Fig. 2 comparing (10,10) GPB and (10,10) SWNT systems for iron (vanadium) in the upper (lower) panel. The transmission for the (10,10) SWNT with iron (vanadium) adatom shown in the upper (lower) panel. As for the (2,2) GPB system, the minority spin channels are suppressed in the case of iron, whereas the majority channels are suppressed for vanadium.

It is instructive to compare the situation to the adatom coupling to a single benzene ring.<sup>39</sup> In this case it is found that the field splits the  $3d$  levels to a singlet A1 ( $3d_{3z^2-r^2}$ ) and two doublets, of E1 ( $3d_{zx}$ ,  $3d_{yz}$ ) and E2 ( $3d_{xy}$ ,  $3d_{x^2-y^2}$ ) symmetry. The E1 states hybridize most strongly with the  $\pi$  system of the ring and form antibonding states at higher energies than the corresponding antibonding states of the A1 and E2 system. It is these hybridizations we observe as Fano antiresonances involving mainly the adatom  $d$  states. The infinite graphene sheet will have the same symmetry as the benzene ring, and we therefore, expect a splitting of the two E1 states, as well as the two E2 states, to approach zero.

## VI. LARGE SWNT COMPARISON

Having understood the scattering mechanism in our small GPB system we now turn to the results for the more realistic (10,10) armchair SWNT. We present in Fig. 7 the transmission, channel transmissions, and PDOS for the adatom on a (10,10) GPB, and the (10,10) SWNT, corresponding to the results in Fig. 2 for the narrow GPB system. Results for the iron (vanadium) adatom are shown in the upper (lower) panel. Notice that the energy window around  $E_F$ , where only two bands conduct, is smaller compared to the (2,2) GPB system due to the increase in system size. Similar to the (2,2) GPB system we find again scattering of mainly one spin type, which is as before minority spin for iron and majority spin for vanadium. The correspondence between  $d$ -orbital PDOS and scattering of Bloch state bands follow here clearly what we described in Sec. IV. As expected from the discussion above we clearly observe that the (10,10) GPB system has almost degenerate “E1” ( $3d_{zx}$ ,  $3d_{yz}$ ) resonances, and likewise for the “E2” ( $3d_{xy}$ ,  $3d_{x^2-y^2}$ ) resonances.

Again we note that it is the minority (majority) spin which is mainly scattered around  $E_F$  in both GPB and SWNT. However, the curvature introduces a remarkably strong splitting of the “E1” and “E2” states compared to the flat GPB. This is especially the case for the iron adatom and could be related to the fact that this atom is located closer to the SWNT and, thus, effectively is more affected by the curvature, compared to the vanadium case. One must consider the influence of curvature on charge transfer both from adatom to host, as well as between orbitals on the adatom, since this may greatly affect the PDOS profile of the adatom. Calculations on a single passivated benzene ring with adatom show that the  $4s$ - to  $3d$ -orbital transfer is decreased by curvature probably since two of the closest carbon atoms are further away from the adatom. However, we do not see evidence hereof in the Mulliken data from the (10,10) systems. A more detailed understanding of the charge transfer and its dependence on curvature is yet to be understood in detail. Calculations with a better basis set are needed to obtain more exact understanding of the electronic structure.

## VII. CONCLUSION

We have described spin-polarized zero-bias transport calculations for armchair carbon nanotubes with adsorbed single iron or vanadium atoms. We find a significant difference between transmissions of majority and minority spin. The presence of the metal adatoms causes spin-dependent closing of the conduction channels at certain energies. The mechanism is due to Fano antiresonances related to the particular  $d$  states close to the Fermi energy. Only  $d$  orbitals with a symmetry matching the symmetry of the Bloch band solutions take part in the scattering. The scattered spin type (minority or majority spin) can be explained by the filling of the  $3d$  orbitals via Hund’s rule. A simple tight-binding model qualitatively reproduces the *ab initio* findings. The scattering mechanism observed for the GPB system is shown also to apply to a large diameter SWNT and to be insensitive to adatom distance to tube or sheet and is, therefore, a very robust effect. The tube curvature introduces a significant splitting of the two “E1” and two “E2” states. Curvature also causes different charge transfers to occur between  $4s$  and  $3d$  orbitals on the adatom, as well as between adatom and tube or sheet. This causes shifts in the PDOS profiles of the  $3d$  orbitals resulting in different transmission for SWNT and GPB systems.

## ACKNOWLEDGMENTS

The authors would like to thank Jeremy Taylor for useful discussions. Computational resources were provided by the Danish Center for Scientific Computations (DCSC). A.P.J. is grateful to the FiDiPro program of the Finnish Academy for support during the final stages of this work. K.S. acknowledges support from the Danish Council for Production and Technology (FTP) under Grant No. 26-04-0181 Atomic scale modeling of emerging electronic devices. J.A.F. acknowledges support from the Danish Agency for Science Technology and Innovation.

\*Corresponding author. jof@mic.dtu.dk

<sup>1</sup>P. Avouris, Z. Chen, and V. Perebeinos, *Nat. Nanotechnol.* **2**, 605 (2007).  
<sup>2</sup>K. S. Novoselov, A. K. Geim, S. V. Morozov, D. Jiang, M. I. Katsnelson, I. V. Grigorieva, S. V. Dubonos, and A. A. Firsov, *Nature (London)* **438**, 197 (2005).  
<sup>3</sup>A. Geim and K. Novoselov, *Nature Mater.* **6**, 183 (2007).  
<sup>4</sup>F. Schedin *et al.*, *Nature Mater.* **6**, 652 (2007).  
<sup>5</sup>G. Prinz, *Science* **282**, 1660 (1998).  
<sup>6</sup>S. Wolf *et al.*, *Science* **294**, 1488 (2001).  
<sup>7</sup>I. Žutić, J. Fabian, and S. Das Sarma, *Rev. Mod. Phys.* **76**, 323 (2004).  
<sup>8</sup>J. R. Hauptmann, J. Paaske, and P. E. Lindelof, *Nat. Phys.* **4**, 373 (2008).  
<sup>9</sup>P. O. Lehtinen, A. S. Foster, Y. Ma, A. V. Krasheninnikov, and R. M. Nieminen, *Phys. Rev. Lett.* **93**, 187202 (2004).

<sup>10</sup>H. Kumazaki and D. S. Hirashima, *J. Phys. Soc. Jpn.* **76**, 064713 (2007).  
<sup>11</sup>E. J. Duplock, M. Scheffler, and P. J. D. Lindan, *Phys. Rev. Lett.* **92**, 225502 (2004).  
<sup>12</sup>S. Okada and A. Oshiyama, *Phys. Rev. Lett.* **87**, 146803 (2001).  
<sup>13</sup>H. Lee, Y.-W. Son, N. Park, S. Han, and J. Yu, *Phys. Rev. B* **72**, 174431 (2005).  
<sup>14</sup>B. Fagan, R. Mota, A. da Silva, and A. Fazzio, *Physica B* **340-342**, 982 (2003).  
<sup>15</sup>B. Fagan, R. Mota, A. da Silva, and A. Fazzio, *J. Phys.: Condens. Matter* **16**, 3647 (2004).  
<sup>16</sup>S. B. Fagan, R. Mota, A. J. R. da Silva, and A. Fazzio, *Phys. Rev. B* **67**, 205414 (2003).  
<sup>17</sup>D. M. Duffy and J. A. Blackman, *Phys. Rev. B* **58**, 7443 (1998).  
<sup>18</sup>Y. Mao, J. Yuan, and J. Zhong, *J. Phys.: Condens. Matter* **20**, 115209 (2008).

- <sup>19</sup>C.-K. Yang, J. Zhao, and J. P. Lu, Phys. Rev. Lett. **90**, 257203 (2003).
- <sup>20</sup>Y. J. Kang, J. Choi, C. Y. Moon, and K. J. Chang, Phys. Rev. B **71**, 115441 (2005).
- <sup>21</sup>T. Kishi, M. David, A. Wilson, H. Nakanishi, and H. Kasai, Jpn. J. Appl. Phys., Part 1 **46**, 1788 (2007).
- <sup>22</sup>M. Monthieux, Carbon **40**, 1809 (2002).
- <sup>23</sup>C. Zhang, L. Wang, and H. Cheng, J. Chem. Phys. **124**, 201107 (2006).
- <sup>24</sup>B. Wang, Y. Zhu, W. Ren, J. Wang, and H. Guo, Phys. Rev. B **75**, 235415 (2007).
- <sup>25</sup>T. Martins, R. Miwa, A. da Silva, and A. Fazzio, Phys. Rev. Lett. **98**, 196803 (2007).
- <sup>26</sup>L. Rosales, M. Pacheco, Z. Barticevic, A. Latge, and P. A. Orellana, Nanotechnology **19**, 065402 (2008).
- <sup>27</sup>J. M. Soler, E. Artacho, J. D. Gale, A. Garcia, J. Junquera, P. Ordejon, and D. Sanchez-Portal, J. Phys.: Condens. Matter **14**, 2745 (2002).
- <sup>28</sup>J. P. Perdew, K. Burke, and M. Ernzerhof, Phys. Rev. Lett. **77**, 3865 (1996).
- <sup>29</sup>M. Brandbyge, J.-L. Mozos, P. Ordejon, J. Taylor, and K. Stokbro, Phys. Rev. B **65**, 165401 (2002).
- <sup>30</sup>Y. Yagi, T. M. Briere, M. H. F. Sluiter, V. Kumar, A. A. Farajian, and Y. Kawazoe, Phys. Rev. B **69**, 075414 (2004).
- <sup>31</sup>C. T. White and J. W. Mintmire, J. Phys. Chem. B **109**, 52 (2005).
- <sup>32</sup>M. Koleini, M. Paulsson, and M. Brandbyge, Phys. Rev. Lett. **98**, 197202 (2007).
- <sup>33</sup>U. Fano, Phys. Rev. **124**, 1866 (1961).
- <sup>34</sup>J. U. Nockel and A. D. Stone, Phys. Rev. B **50**, 17415 (1994).
- <sup>35</sup>A. R. P. Rau, Phys. Scr. **69**, C10 (2004).
- <sup>36</sup>Z. Zhang and V. Chandrasekhar, Phys. Rev. B **73**, 075421 (2006).
- <sup>37</sup>M. Paulsson and M. Brandbyge, Phys. Rev. B **76**, 115117 (2007).
- <sup>38</sup>W. A. Harrison, *Electronic Structure and the Properties of Solids* (Dover, New York, 1989).
- <sup>39</sup>V. V. Maslyuk, A. Bagrets, V. Meded, A. Arnold, F. Evers, M. Brandbyge, T. Bredow, and I. Mertig, Phys. Rev. Lett. **97**, 097201 (2006).